

# ORCA - Online Research @ Cardiff

This is an Open Access document downloaded from ORCA, Cardiff University's institutional repository:https://orca.cardiff.ac.uk/id/eprint/181886/

This is the author's version of a work that was submitted to / accepted for publication.

Citation for final published version:

Niu, Shanshan, Qian, Lei-lei, Wang, Yin-yuan, Chu, Guoxiang, Wu, Yingluo, Yang, Ji and Qi, Haifeng 2025. Cu-doped activated Co3O4: tandem site efficient electrocatalytic reduction of nitrate to ammonia.

ChemistrySelect 10 (40), e04759. 10.1002/slct.202504759

Publishers page: https://doi.org/10.1002/slct.202504759

## Please note:

Changes made as a result of publishing processes such as copy-editing, formatting and page numbers may not be reflected in this version. For the definitive version of this publication, please refer to the published source. You are advised to consult the publisher's version if you wish to cite this paper.

This version is being made available in accordance with publisher policies. See http://orca.cf.ac.uk/policies.html for usage policies. Copyright and moral rights for publications made available in ORCA are retained by the copyright holders.



# Cu-doped activated Co<sub>3</sub>O<sub>4</sub>: Tandem site efficiently electrocatalytic reduction of nitrate to ammonia

Shanshan Niu\*[a], Lei-lei Qian\*[a], Yin-yuan Wang[a], Guoxiang Chu[a], Yingluo Wu[a], Ji Yang\*[b], Haifeng Qi\*[c]

[a] Dr. S. Niu, Dr. L. Qian, Y. Wang, G. Chu, Y. Wu

School of Life Sciences and Chemical Engineering

Jiangsu Second Normal University

Nanjing 211200, China

E-mail: nss1220@jssnu.edu.cn

[b] Dr. Ji Yang

CAS Key Laboratory of Molecular Nanostructure and Nanotechnology

Institute of Chemistry, Chinese Academy of Sciences (CAS)

Beijing 100190, China

E-mail: yangji@iccas.ac.cn

[c] Dr. Haifeng Qi

Max Planck-Cardiff Centre on the Fundamentals of Heterogeneous Catalysis FUNCAT, Translational Research Hub

Cardiff University

Maindy Road, Cardiff CF24 4HQ, UK

E-mail: qih11@cardiff.ac.uk

Supporting information for this article is given via a link at the end of the document.

**Abstract:** The electroreduction of nitrate (NO<sub>3</sub><sup>-</sup>) into ammonia (NH<sub>3</sub>) presents a promising avenue for sustainable ammonia synthesis. In this study, we construct electrocatalyst with tandem sites that integrates highly dispersed Cu with Co<sub>3</sub>O<sub>4</sub> by self-sacrifice strategy using MOF as a template, which significantly improves NH<sub>3</sub> production. The resulting Cu-Co<sub>3</sub>O<sub>4</sub> catalyst achieves a NH<sub>3</sub> yield rate of 7.25 mg h<sup>-1</sup> cm<sup>-2</sup> and Faradaic efficiency (FE) of 95%. Mechanism research shows that Cu enhances NO<sub>3</sub><sup>-</sup> adsorption, the synergy between Cu and Co<sub>3</sub>O<sub>4</sub> increases the electrochemical active area, reduces charge transfer resistance, inhibits hydrogen evolution reaction. The confinement effect of Co<sub>3</sub>O<sub>4</sub> effectively ensures the stability of Cu<sup>2+</sup> in the electrocatalytic reduction reaction process. This work offers valuable insights into the tandem NO<sub>3</sub><sup>-</sup> reduction pathway in heterostructures, providing a foundation for optimizing catalysts and advancing sustainable NH<sub>3</sub> synthesis.

#### Introduction

Applications of ammonia (NH<sub>3</sub>) span numerous key industries including agriculture, energy and national defense. The industrial synthesis of ammonia of Haber-Bosch process utilizes nitrogen and hydrogen as feedstocks, consumes fossil fuels and emits carbon dioxide, the development of new sustainable synthetic ammonia technologies are of profound importance. <sup>1-4</sup> As a cutting-edge technology, electrocatalytic nitrogen reduction can directly synthesize ammonia from water and nitrogen at room temperature and pressure, but faces bottlenecks such as the high binding energy of N  $\equiv$  N triple bond (941 kJ mol<sup>-1</sup>), low nitrogen solubility, severely limit activity and selectivity. <sup>5-8</sup> Recently, the electrochemical ammonia synthesis using nitrate (NO<sub>3</sub><sup>-</sup>) as the nitrogen source has shown significant improvement in both yield and selectivity. <sup>9-12</sup> Nitrate with high water solubility, can be obtained from industrial wastewater, domestic sewage and low-temperature plasma activated nitrogen. The conversion of nitrate to ammonia can bypass the bottleneck of high binding energy of N<sub>2</sub> (N=O bond energy 204 kJ mol<sup>-1</sup>), overcome the high energy consumption and high pollution limitations of the Haber-Bosch process, and address the environmental pollution issue of nitrate in water. <sup>13-17</sup>

Electrocatalyst plays a key role in improving energy efficiency and performance. The NO<sub>3</sub>- reduction faces the following challenges: (a) The competitive hydrogen evolution reaction (HER) reduces Faraday efficiency; (b) The complex process of multi electron/proton transformation; (c) The adsorption of key intermediates is difficult to optimize resulting in low selectivity of NH<sub>3</sub>. Copper (Cu)-based electrocatalysts can undergo resonance hybridization with the  $\pi$  orbitals of NO<sub>3</sub>- due to the unique d-orbital configuration, have been extensively investigated for NO<sub>3</sub><sup>-</sup> reduction due to remarkable absorbing capacity towards NO<sub>3</sub><sup>-</sup>.18, 19 Pure copper catalysts have been proven to spontaneous oxidation dissolution and surface deactivation, the concentration of ammonia increases as the concentration of nitrate decreases in the solution, leading to the inevitable reaction between copper and ammonia to form copper ammonia complexes.<sup>20</sup> Moreover, due to weak hydrogen adsorption ability of Cu, the intermediates (\*NO<sub>2</sub>, \*NO, \*N, etc.) produced by NO<sub>3</sub>- reduction cannot be hydrogenated in a timely manner, thereby limiting the efficiency of ammonia synthesis. 21-25 One of strategies resolved the above bottlenecks involves altering the intrinsic activity of Cu by forming alloys and heterostructures such as Cu@C, Ru-Cu nanowires and Cu/Cu<sub>2</sub>O.<sup>26-28</sup> Another one is the construction of tandem catalysts to facilitate the reaction through a cascade pathway to disrupt the scaling relationship of intermediates over a single active site. Electrocatalytic  $NO_3^-$  reduction can be divided into two stages with  $NO_3^- \rightarrow NO_2^-$  and  $NO_2^- \rightarrow NH_3^{-29,30}$  The crux of matter lies in the selection of two active sites to facilitate selective catalysis at various stages. Previous research has demonstrated that intrinsic Co-based catalysts can effectively convert NO2- to NH3, but are not satisfactory for reduction of NO<sub>3</sub><sup>-</sup> to NH<sub>3</sub>, likely because of weak affinity for NO<sub>3</sub><sup>-</sup>. When a Co-based catalyst integrates with Cu, exhibits enhanced NO<sub>3</sub> reduction activity.<sup>31</sup> In this study, we engineered a highly dispersed Cu-doped Co<sub>3</sub>O<sub>4</sub> core-shell nanostructure using metal-organic framework (MOF) as template by pyrolysis in Air

atmosphere, and utilizing the confinement effect of ZIF-67 to prevent Cu aggregation. The Air atmosphere calcination avoids excessive reduction or Cu aggregation that may be caused by reducing atmosphere, and accurately achieves the coexistence and synergy of Cu<sup>2+</sup> and Co<sup>2+</sup>/Co<sup>3+</sup>. The strong metal carrier interaction of Co<sub>3</sub>O<sub>4</sub> further anchors Cu<sup>2+</sup>, forming a stable Cu-O-Co interface structure. When utilized as NO<sub>3</sub><sup>-</sup> reduction electrocatalysts, obtained Cu-Co<sub>3</sub>O<sub>4</sub> catalysts display a high NH<sub>3</sub> yield rate of 7.25 mg h<sup>-1</sup> cm<sup>-2</sup> at -0.9 V vs. RHE and a commendable Faradaic efficiency (FE) of 95% at -0.7 V vs. RHE. Mechanistic studies suggest that Cu and Co<sub>3</sub>O<sub>4</sub> could selectively catalyze the reduction of NO<sub>3</sub><sup>-</sup> to NO<sub>2</sub><sup>-</sup> and subsequently NO<sub>2</sub><sup>-</sup> to NH<sub>3</sub>. Cu<sup>2+</sup> increases the electrochemical active area, the multi valent states of Cu<sup>+</sup>/Co<sup>2+</sup>/Co<sup>3+</sup> construct electron transfer channels, reduce charge transfer resistance, Cu<sup>2+</sup> inhibits competitive HER, enhances nitrate adsorption, significantly accelerating the reaction kinetics. The confinement effect of Co<sub>3</sub>O<sub>4</sub> effectively ensures the stability of Cu<sup>2+</sup> in the electrocatalytic reduction reaction process.

#### **Results and Discussion**

The Cu-Co<sub>3</sub>O<sub>4</sub> electrocatalyst is constructed by MOF-derived template strategy (Figure 1): (1) Cobalt ions coordinate with 2-methylimidazole to form metal-organic framework of ZIF-67 at room temperature; (2) Copper precursors are introduced in ZIF-67 and subjected to pyrolysis at 450°C in the Air atmosphere to obtain Cu-Co<sub>3</sub>O<sub>4</sub>. The phase composition of ZIF-67, Cu-ZIF-67, Cu-Co<sub>3</sub>O<sub>4</sub> and Co<sub>3</sub>O<sub>4</sub> are characterized by X-ray diffraction (XRD). As depicted in Figure S1, Cu-ZIF-67 exhibits identical diffraction peaks of ZIF-67, while all peaks of both Cu-Co<sub>3</sub>O<sub>4</sub> and Co<sub>3</sub>O<sub>4</sub> samples correspond to characteristic peaks of Co<sub>3</sub>O<sub>4</sub> (PDF # 43-1003), and no characteristic peaks of copper containing species are observed.<sup>32</sup> The scanning electron microscope (SEM) images reveal the dodecahedral morphology of ZIF-67 sample with diameters of approximately 1 µm (Figure S2). The Cu-ZIF-67 precursor samples, synthesized through the addition of copper salt, retain dodecahedral morphology with a rough and contracted surface, and energy-dispersive X-ray spectroscopy (EDS) mapping confirms the presence of copper (Figure S3). When the Cu-ZIF-67 precursor is used as a sacrificial template and subjected to pyrolysis under air at 450 °C, a temperature exceeding the decomposition temperatures determined by thermogravimetric analysis (Figure S4), the morphology undergo significant changes (Figure 1b and S5). It is speculated that the organic ligands of metal-organic framework decompose and the metal sites undergo a redox reaction during heat treatment, across which the gas generated by Cu-ZIF-67 precursor decomposition is continuously released to leave hollow interior behind, integrating into the Cu-doped Co<sub>3</sub>O<sub>4</sub> core-shell structure nanocages structure with internal cavity. Element mapping indicates the uniformed dispersion of Co, O and Cu element, with a 9 wt.% content of Cu confirmed by inductively coupled plasma spectrometer (ICP). The nanostructures are further verified by the transmission electron microscopy (TEM) (Figure 1c), show that the interior and outer structure is constructed from interconnected nanosheets. The highresolution transmission electron microscopy (HRTEM) images (Figures 1d and e) show that the lattice fringes with spacings of 0.236 nm corresponded to the (222) plane of Co<sub>3</sub>O<sub>4</sub>, respectively, larger than that of pristine Co<sub>3</sub>O<sub>4</sub> (0.233 nm), indicative of interplanar expansion due to Cu's larger atomic radius (Figure S6). Figure 2f shows the EDS mapping image of Cu-Co<sub>3</sub>O<sub>4</sub>, Co and O element are distributed homogeneously throughout the region, the signal intensity of Cu is very uniform with enhancement in the outer locates.

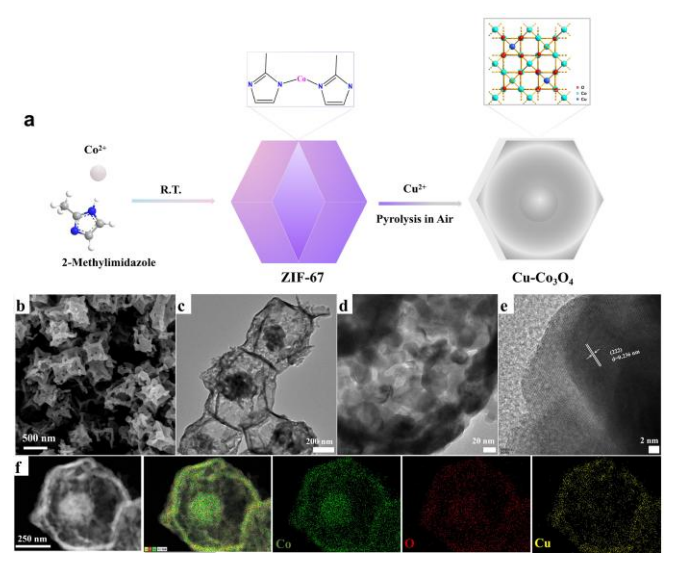


Figure 1. (a) Schematic illustration for the formation of Cu-Co<sub>3</sub>O<sub>4</sub>; (b) SEM images; (c) TEM images; (d, e) HR-TEM images; (f) EDS mapping of 0.1Cu-Co<sub>3</sub>O<sub>4</sub> samples.

The vibration peaks at 189.2, 468.3, 513, 609 and 683.5 cm<sup>-1</sup> correspond to the characteristic Raman active modes of  $Co_3O_4$  vibration mode of  $F_{2g}^{(3)}$ ,  $E_{1g}$ ,  $F_{2g}^{(2)}$ ,  $F_{2g}^{(1)}$ , and  $A_{1g}$ , respectively. Among them, the  $A_{1g}$  and  $F_{2g}^{(3)}$  active modes represent octahedral sites ( $CoO_6$ ) and tetrahedral sites ( $CoO_4$ ) of  $Co_3O_4$  (Figure 2a). In particular, the  $A_{1g}$  peak of Cu- $Co_3O_4$  shows a blue shift due to the lattice distortion derived from Cu doping.  $^{33}$  The surface composition and valence states of  $Co_3O_4$  and Cu- $Co_3O_4$  are further identified by X-ray photoelectron spectroscopy (XPS). The Cu 2p XPS spectrum (Figure 2b) features two distinct peaks at 934.1 eV and 953.9 eV, correlating to Cu 2p<sub>3/2</sub> and 2p<sub>1/2</sub> states of  $Cu^{2+}$ , along with satellite peaks. $^{34}$  In parallel, the high-resolution Co 2p spectra shows peaks at approximately 796.59 eV, 794.8 eV, 781.58 eV and 779.80 eV, denoting  $Co^{2+}/Co^{3+}$  oxidation states augmented by satellite peaks. $^{35}$  Notably, the integration of Cu into  $Co_3O_4$  induces a higher energy shift in Co 2p peaks compared with  $Co_3O_4$ , contributes to the optimal regulation of electronic structures and further improves reaction rate of interfacial catalytic process (Figure 2c). $^{36}$  Additionally, the O 1s spectrum of Cu-Co3O<sub>4</sub> could be split into six peaks, attributed to Co-O, Cu-O, surface hydroxyl (M-O-H), low oxygen-coordinated defect sites ( $V_O$ ), surface oxygen ( $O_{Surf}$ ) and adsorbed oxygen ( $O_{adv}$ ), respectively. Together, these results further confirm the effective incorporation of Cu into the  $Co_3O_4$  and formation of Cu-O-Co heterogeneous interface (Figure 2d). $^{37}$ , 38

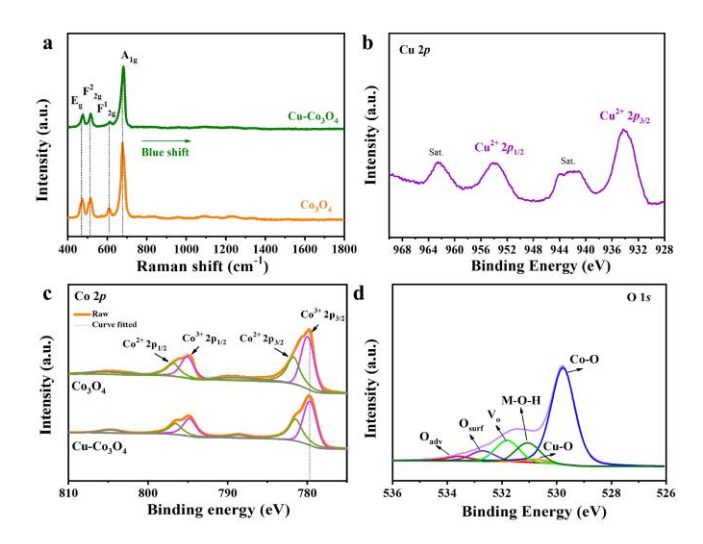


Figure 2. (a) Raman spectra and (b, c, d) XPS spectra in the Cu 2p, Co 2p and O 1s regions of Cu-Co<sub>3</sub>O<sub>4</sub> and Co<sub>3</sub>O<sub>4</sub>.

The electrocatalytic performance of  $NO_3^-$  reduction reaction is evaluated in an H-type cell with 0.1 M KOH + 0.1 M KNO<sub>3</sub> electrolyte. As shown in Figure 3a, the linear sweep voltammetry (LSV) curves of Cu-Co<sub>3</sub>O<sub>4</sub> samples show higher current density in the  $NO_3^-$  containing electrolyte compared with that of electrolyte without  $NO_3^-$ , indicating the occurrence of effective  $NO_3^-$  reduction reaction. Moreover, the current density of Cu-Co<sub>3</sub>O<sub>4</sub> catalyst is higher than that of  $Co_3O_4$  catalyst in the presence of  $NO_3^-$ , indicated that the introduction of copper is more conducive to promoting the conversion of  $NO_3^-$ . When perform  $NO_3^-$  reduction reaction at -0.6 V to -1 V vs. RHE for 0.5 h, the Faradaic efficiency (FE) of Cu-Co<sub>3</sub>O<sub>4</sub> catalyst increases with potential up to -0.7 V vs. RHE, and decreased at more negative potential results from the enhanced competing hydrogen evolution reaction (HER). Cu-Co<sub>3</sub>O<sub>4</sub> catalyst offers the highest  $NH_3$  yield rate of 7.25 mg h<sup>-1</sup> cm<sup>-2</sup> at -0.9 V vs. RHE and FE of 95% at -0.7 V vs. RHE (Figures 3b and 3c), higher than those of  $Co_3O_4$  catalyst (5.98 mg h<sup>-1</sup> cm<sup>-2</sup> and 88%), exceeding many of reported Cu- or Co-based  $NO_3^-$  reduction electrocatalysts (Figure 3d), indicating the high electrocatalytic  $NO_3^-$  reduction activity of obtained Cu-Co<sub>3</sub>O<sub>4</sub> catalyst.<sup>39-47</sup>

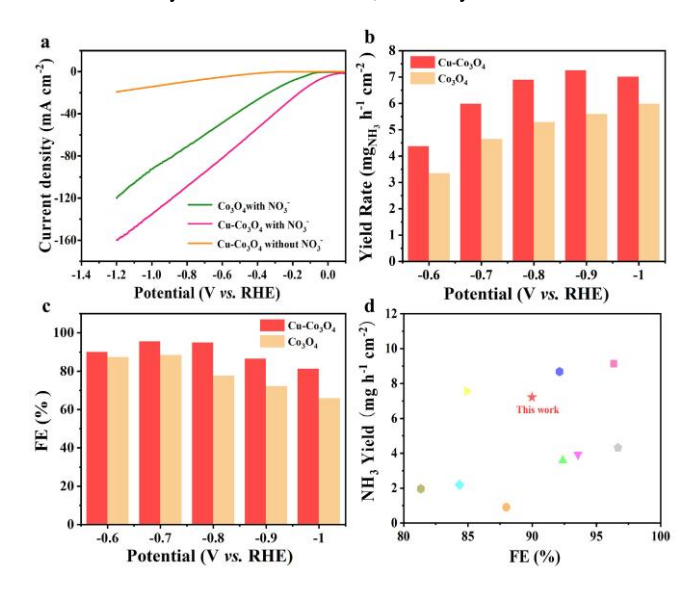


Figure 3. (a) LSV curves of  $Cu-Co_3O_4$ ,  $Co_3O_4$  in 0.1 M KOH aqueous solution with and without 0.1 M KNO<sub>3</sub>; (b) NH<sub>3</sub> yield rates and (c) FEs for NH<sub>3</sub> over  $Cu-Co_3O_4$ ,  $Co_3O_4$  in 0.1 M KOH aqueous solution with 0.1 M KNO<sub>3</sub> at each given potential; (d) Comparison of NH<sub>3</sub> yield rates and FEs at different potentials for recently reported state-of-the-art electrocatalysts.

Additionally, long-term electrocatalytic tests over  $Cu-Co_3O_4$  samples are performed at potential of -0.7 V vs. RHE. As observed in Figure 4a and 4b,  $Cu-Co_3O_4$  samples display a relatively stable FEs exceeding 90% for 10 cycles and could running for 72 h, indicating good electrocatalytic stability. The XPS test results of  $Cu-Co_3O_4$  samples after 72 h stability measurement indicate that copper mainly exists in the form of  $Cu^{2+}$ , which verifies stabilizing effect of  $Co_3O_4$  towards  $Cu^{2+}$  (Figure 4c and 4d).

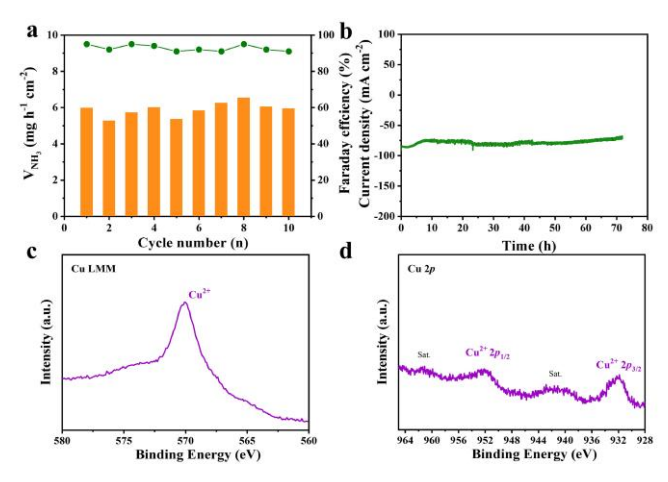


Figure 4. (a) The consecutive cycling stability test and (b) chronoamperometry measurement for 72 h -0.7 V vs. RHE; (c) Cu LMM and Cu 2p spectra after 72 h long-time stability measurement of Cu-Co<sub>3</sub>O<sub>4</sub> at -0.7 V vs. RHE.

To further clarify the synergy effect between Cu and  $Co_3O_4$  for  $Cu-Co_3O_4$ , a series of control experiments are conducted. Figure 6a shows the adsorption capacities ( $q_e$ ) of  $Cu-Co_3O_4$  and  $Co_3O_4$  for  $NO_3^-$ . Larger  $q_e$  for  $NO_3^-$  of  $Cu-Co_3O_4$  indicates that the introduction of copper can effectively enhance the adsorption capacity of  $NO_3^-$  (Figure 5a). Because  $NO_2^- \to NH_3$  is a second stage of  $NO_3^- \to NH_3$ , the content of  $NO_2^-$  over  $Cu-Co_3O_4$  and  $Co_3O_4$  catalysts after  $NO_3^-$  reduction reaction and performance of electrocatalytic  $NO_2^-$  reduction to ammonia are also performed. At potentials of -0.7 V vs. RHE, the  $Cu-Co_3O_4$  samples show more less  $NO_2^-$  and higher  $NH_3$  yield rate for  $NO_2^-$  reduction than that of  $Co_3O_4$ , suggest that the  $Cu-Co_3O_4$  is more active for  $NO_2^- \to NH_3$  (Figure 5b and 5c). Therefore, the  $NO_3^-$  reduction could probably proceed in a tandem catalysis pathway over  $Cu-Co_3O_4$ : the  $NO_3^- \to NO_2^-$  conversion over Cu then  $NO_2^- \to NH_3$  conversion over  $Co_3O_4$ . An appropriate amount of Cu is required to achieve the highest  $NH_3$  selectivity by cooperating with  $Co_3O_4$  based on the study for regulating the amount of copper added (Figure S8). The possible ammonia contamination is also excluded from the bare glass carbon electrode, 0.1 M KOH electrolyte and open circuit potential controlled variable experiment, respectively (Figure S9).

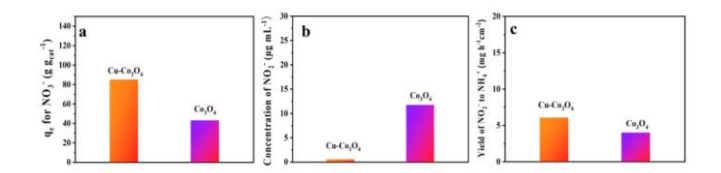


Figure 5. (a) Adsorption capacities of  $Cu-Co_3O_4$  and  $Co_3O_4$  for  $NO_3$ ; (b) Concentration of  $NO_2$  of  $Cu-Co_3O_4$  after testing 0.5 h; (c) Yield rates of  $NO_2$  to  $NH_3$  of  $Cu-Co_3O_4$  after testing 0.5 h at -0.7 V vs. RHE.

In addition, the larger double-layer capacitance ( $C_{dl}$ ) for  $Cu-Co_3O_4$  indicates the more exposed electrochemical activity sites than that of  $Co_3O_4$  (Figure 6a).<sup>48</sup> The electrochemical impedance spectroscopy (EIS) test results show the smaller semi-circular arc of  $Cu-Co_3O_4$ , unveils the better conductivity and faster electron transfer kinetics for reduction of  $NO_3^-$  (Figure 6b).<sup>49</sup> To further investigate the  $NO_3^-$  reduction reaction pathway of the  $Cu-Co_3O_4$ 

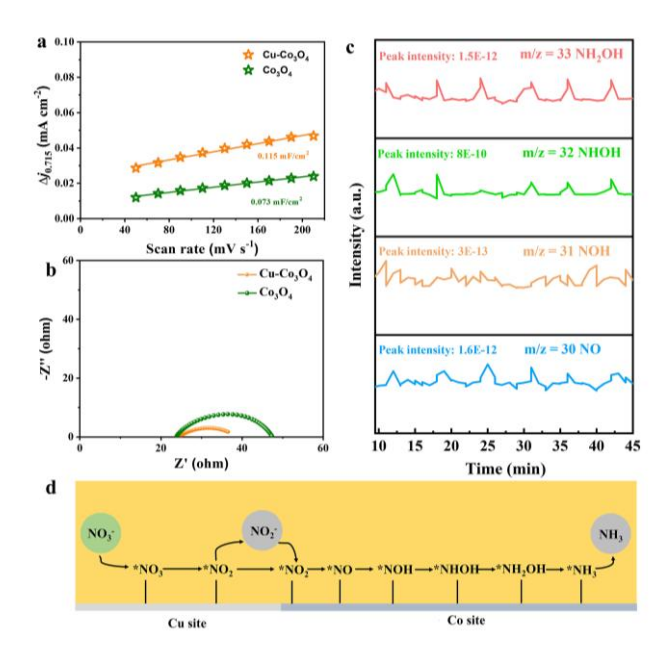


Figure 6. (a) Plots of current density versus scan rates for Cu-Co<sub>3</sub>O<sub>4</sub> and Co<sub>3</sub>O<sub>4</sub>; (b) Nyquist curves of Cu-Co<sub>3</sub>O<sub>4</sub> and Co<sub>3</sub>O<sub>4</sub>; (c) DEMS measurements of NO<sub>3</sub><sup>-</sup> reduction reaction over Cu-Co<sub>3</sub>O<sub>4</sub>; (d) NO<sub>3</sub><sup>-</sup> reduction pathway over Cu-Co<sub>3</sub>O<sub>4</sub>. catalyst, reaction intermediates and products are monitored by Online differential electrochemical mass spectrometry (DEMS).<sup>50</sup> The m/z signals 30, 31, 32 and 33 corresponding to \*NO, \*NOH, \*NHOH and \*NH<sub>2</sub>OH could be detected. Based on the above, the possible reaction pathways for conversion of NO<sub>3</sub><sup>-</sup> to NH<sub>3</sub> could be speculated (Figure 6d). The \*NO<sub>3</sub> intermediate undergoes a series of reactions resulting in the generation of \*NO<sub>2</sub> on Cu sites, and further leading to the formation of \*NO, \*NOH, \*NHOH, \*NH<sub>2</sub>OH intermediate, and finally obtain NH<sub>3</sub> product on Co sites.

In situ electrochemical impedance spectroscopy (EIS) is employed to investigate the reaction kinetics of water dissociation and NO<sub>3</sub><sup>-</sup> reduction reaction. For the electrolyte without NO<sub>3</sub><sup>-</sup>, Cu-Co<sub>3</sub>O<sub>4</sub> exhibits a characteristic peak centered in the high-frequency region (10<sup>2</sup>-10<sup>3</sup> Hz) (Figure 7a). As the potential increases, the peak shifts towards the high-frequency region and peak intensity decrease obviously, related to the non-uniform charge distribution caused by HER. For the electrolyte with NO<sub>3</sub><sup>-</sup>, a new kinetic process appears in the intermediate frequency range, originates from the reduction reaction of NO<sub>3</sub><sup>-</sup> on the Cu-Co<sub>3</sub>O<sub>4</sub> catalyst surface (Figure 7b). Compared with Co<sub>3</sub>O<sub>4</sub>, the phase angle intensity of Cu-Co<sub>3</sub>O<sub>4</sub> significantly decreases, indicating a faster electron transfer rate and more charges involved in the Faraday process, which promotes the hydrolysis dissociation process and enables NO<sub>3</sub><sup>-</sup> to easily capture \*H to form ammonia, thereby accelerating the nitrate reduction reaction rate. In addition, the peak position of the phase angle shifts towards lower frequencies, further confirming that the copper load can effectively suppress Heyrovsky step and prevent hydrogen evolution (Figure 7c and 7d).<sup>51-55</sup>

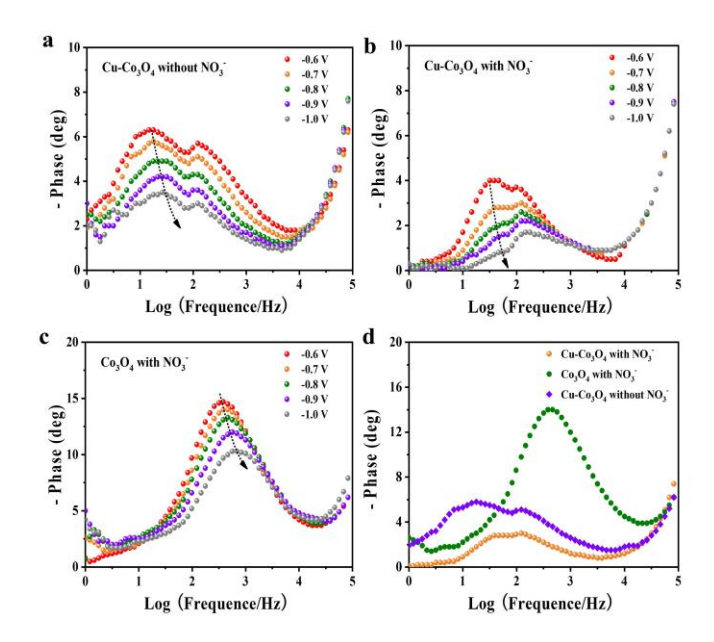


Figure 7. Bode phase plots of  $Cu-Co_3O_4$  at different potentials (a) 0.1 M KOH; (b) 0.1 M KOH with 0.1 M NO<sub>3</sub><sup>-</sup>; (c) Bode phase plots of  $Co_3O_4$  at varied potentials in 0.1 M KOH + 0.1 M NO<sub>3</sub><sup>-</sup>; (d) Bode phase plots of  $Cu-Co_3O_4$  and  $Co_3O_4$  in 0.1 M KOH with or without  $NO_3$ <sup>-</sup>-0.7 V vs. RHE.

## Conclusion

In summary, we prepare a highly efficient  $Cu-Co_3O_4$  as a tandem electrocatalyst for  $NO_3^-$  reduction to  $NH_3$ . The catalyst displays an outstanding electrocatalytic activity with a maximum  $NH_3$  yield rate of 7.25 mg h<sup>-1</sup> cm<sup>-2</sup> and the highest Faradaic efficiency of 95% in alkaline electrolyte. It can be speculated that  $NO_3^-$  could be reduced to  $NO_2^-$  over Cu sites,  $NO_2^-$  reduction to  $NH_3$  over  $Co_3O_4$ . Cu doping is beneficial for adsorption and subsequent conversion of  $NO_3^-$ , while preventing  $H^*$  coupling to form  $H_2$ .  $Co_3O_4$  plays an important role in stabilizing  $Cu^{2+}$  active sites. This work goes beyond simple "doping enhances activity" and reveals the profound mechanism of multi metal site synergistic regulation of electronic structure and reaction pathways, providing important reference for designing next-generation energy and environmental catalytic materials.

## **Supporting Information**

The supporting information provides catalyst synthesis, structural characterization, electrochemical testing, preparation of color developing agent, detailed calculation of FEs and ammonia yield, standard curve equation, XPS spectra, chronoamperometric curves, UV-vis absorption spectra.

## Acknowledgements

This work was supported by has been financed by the Natural Science Foundation of Jiangsu Higher Education Institutions of China (Grant 22KJB150021), high-level talent research of Jiangsu Second Normal University (928201/009), Jiangsu Province Basic Research Program (Natural Science Foundation) (BK20241100), Jiangsu young scientific and technological talents promotion project (JSTJ-2024-398).

#### **Conflict of Interest**

The authors declare no conflict of interest.

# **Data Availability Statement**

The data that support the findings of this study are available in the supplementary material of this article.

**Keywords:** ammonia production • NO<sub>3</sub>- reduction • tandem site • MOF

- 1. W. Chen, Y. Xu, J. Liu, H. Cao, Y. Li, X. Ren, S. Ye, J. Liu and Q. Zhang, *Inorg. Chem. Front.*, 2023, 10, 4901-4917.
- 2. Z. Xi, H. Hu, Q. Chen, M. Ning, S. Wang, H. Yu, Y. Sun, D. W. Wang, H. Jin and H. M. Cheng, *Adv. Funct. Mater.*, **2025**, 35, 2425611.
- 3. J. Zhou, S. Gao and G. Hu, Energy & Fuels, 2024, 38, 6701-6722.
- 4. Y. Xiong, Y. Wang, J. Zhou, F. Liu, F. Hao and Z. Fan, Adv. Mater., 2024, 36, e2304021.
- 5. I. Anis, S. Amin, G. M. Rather and M. A. Dar, Chemistry Select, 2023, 8, e202300993.
- 6. S. Chen, F. Yin, X. He and J. Tan, *ChemistrySelect*, **2023**, 8, e202204988.
- 7. M. S. N. K, C. Sathiskumar and N. S. John, ChemistrySelect, 2023, 8, e202203344.
- 8. S. Niu, L.-L. Qian, P. Du, N. Si, D. Jiang, Y. Feng, B. Huang, X. Gu, Q. Zhao, J. Ji and H. Zhu, *Nano LIFE*, **2022**, 13(1), 1-8.
- 9. X. Zhang, G. Ma, L. Shui, G. Zhou and X. Wang, Chem. Eng. J. 2022, 430, 132666.
- 10. H. Wang, J. Huang, J. Cai, Y. Wei, A. Cao, B. Liu and S. Lu, Small Methods, 2023, 7, e2300169.
- 11. Z. Shen, G. Chen, X. Cheng, F. Xu, H. Huang, X. Wang, L. Yang, Q. Wu and Z. Hu, Sci. Adv., 2024, 10, eadm9325.
- 12. H. Zhang, H. Wang, X. Cao, M. Chen, Y. Liu, Y. Zhou, M. Huang, L. Xia, Y. Wang, T. Li, D. Zheng, Y. Luo, S. Sun, X. Zhao and X. Sun, *Adv. Mater.*, **2024**, 36, e2312746.
- 13. Q. Cheng, S. Liu, Y. He, M. Wang, H. Ji, Y. Huan, T. Qian, C. Yan and J. Lu, Nat. Commun., 2025, 16, 3717.
- 14. J. Wan, J. Yang, N. Yang, Y. Sun, C. Hu, Y. Zhao, X. Xu, H. Qi, X. Li and H. Zhang, *ACS Catal.*, **2025**, 15, 4507-4518.
- 15. G. Zhang, X. Li, K. Chen, Y. Guo, D. Ma and K. Chu, Angew Chem. Int. Ed., 2023, 62, e202300054.
- 16. C. Zhang, Y. Zhang, R. Deng, L. Yuan, Y. Zou, T. Bao, X. Zhang, G. Wei, C. Yu and C. Liu, *Adv. Mater.*, **2024**, 36, e2313844.
- 17. S. Tian, R. Wu, H. Liu, C. Yan, Z. Qi, P. Song, W. J. Chen, L. Song, Z. Wang and C. Lv, *Angew Chem. Int. Ed.*, **2025**. 64. e202510665.
- 18. K. Zhang, Y. Liu, Z. Pan, Q. Xia, X. Huo, O. C. Esan, X. Zhang and L. An, *EES Catalysis*, **2024**, 2, 727-752.
- 19. W. Mei, C.-W. Chang, Z. Li, X. Wang, Y. Qie, Q. Liu, R. C. Davis, Z. Wu, Y. Yue, C. Yang, S. Li, D. Han, Q.-H. Yang, Z. Feng and Z. Weng, *Adv. Mater.*, **2025**, n/a, 2507363.
- 20. J. Y. Fang, J. L. Fan, S. B. Liu, S. P. Sun and Y. Y. Lou, *Materials*, 2023, 16, 4000.
- 21. J. Lan, Z. Wang, C. W. Kao, Y. R. Lu, F. Xie and Y. Tan, Nat. Commun., 2024, 15, 10173.
- 22. C. Sun, Y. Xiao, X. Liu, J. Hu, Q. Zhao, Z. Yin and S. Cao, Inorg. Chem., 2024, 63, 11852-11859.
- 23. Y. Dai, S. Li, X. Li, K. Liu, Y. Guo, H. Li and B. Jiang, Adv. Funct. Mater., 2025, 35, 2420282.
- 24. Z. Li, Z. Shi, Y. Ou, L. Zhong, C. Yan, C. Zhang, K. Song, H. Liu, D. Liu, P. Song, C. Yin, Z. Qi, L. Song and C. Lv, *Angew Chem. Int. Ed.*, **2025**, 64, e202510287.
- 25. Z. Li, Q. Wang, L. Zhong, C. Yan, Z. Shi, Y. Ou, Y. Shang, C. Zhang, S. Tian, H. Liu, D. Liu, P. Song, Z. Qi, L. Song and C. Lv, *Mater. Today*, **2025**, 85, 49-59.
- 26. K. Liu, Z. Sun, X. Peng, X. Liu, X. Zhang, B. Zhou, K. Yu, Z. Chen, Q. Zhou, F. Zhang, Y. Wang, X. Gao, W. Chen and P. Chen, *Nat. Commun.*, **2025**, 16, 2167.
- 27. Y. Wang, W. Zhou, R. Jia, Y. Yu and B. Zhang, Angew Chem. Int. Ed., 2020, 59, 5350-5354.

- 28. Z. Song, Y. Liu, Y. Zhong, Q. Guo, J. Zeng and Z. Geng, Adv. Mater., 2022, 34, e2204306.
- 29. X. Wang, J. J. Wang, H. Hu, C. Yin, L. Y. Chang, Y. Zhu, J. Wang and M. Yang, Adv. Mater., 2025, e2504505.
- 30. X. Ouyang, W. Qiao, Y. Yang, B. Xi, Y. Yu, Y. Wu, J. Fang, P. Li and S. Xiong, *Angew Chem. Int. Ed.*, **2025**, 64, e202422585.
- 31. Y. Liu, J. Wei, Z. Yang, L. Zheng, J. Zhao, Z. Song, Y. Zhou, J. Cheng, J. Meng, Z. Geng and J. Zeng, *Nat. Commun.*, **2024**, 15, 3619.
- 32. D. Liu, L. Qiao, Y. Chen, P. Zhou, J. Feng, C. C. Leong, K. W. Ng, S. Peng, S. Wang, W. F. Ip and H. Pan, *Appl. Catal. B: Environ.* **2023**, 324, 122201.
- 33. F. Yue, W. Duan, R. Li, M. Huang, T. Wei, X. Lv, J. Wu, C. Yang, Y. Lu and Z. Gao, *Appl. Surf. Sci.*, **2024**, 649, 159223.
- 34. R. Wang, S. Jia, L. Wu, L. Zhang, X. Song, X. Tan, C. Zheng, W. Li, X. Ma, Q. Qian, X. Kang, Q. Zhu, X. Sun and B. Han, *Angew Chem. Int. Ed.*, **2025**, 64, e202425262.
- 35. C. Chen, H. Su, L.-N. Lu, Y.-S. Hong, Y. Chen, K. Xiao, T. Ouyang, Y. Qin and Z.-Q. Liu, *Chem. Eng. J.*, **2021**, 408, .127814
- 36. W. Li, K. Liu, S. Feng, Y. Xiao, L. Zhang, J. Mao, Q. Liu, X. Liu, J. Luo and L. Han, *J. Colloid. Interface Sci.*, **2024**, 655, 726-735.
- 37. W. Huang, W. Luo, J. Liu, B. E. Jia, C. Lee, J. Dong, L. Yang, B. Liu and Q. Yan, *ACS Nano*, **2024**, 18(31), 20258-20267.
- 38. H. Zheng, Y. Zhang, Y. Wang, Z. Wu, F. Lai, G. Chao, N. Zhang, L. Zhang and T. Liu, Small, 2023, 19, e2205625.
- 39. Y. Tang, S. Liu, C. Guo, Y. Liu and Z. Tang, Sustain. Energy & Fuels, 2023, 7, 5039-5045.
- 40. X. Zhang, C. Wang, Y. Guo, B. Zhang, Y. Wang and Y. Yu, J. Mater. Chem. A, 2022, 10, 6448-6453.
- 41. H. Wang, Y. Guo, C. Li, H. Yu, K. Deng, Z. Wang, X. Li, Y. Xu and L. Wang, *ACS Appl. Mater. Interfaces*, **2022**, 14, 34761-34769.
- 42. X. He, T. Xie, K. Dong, J. Nan, H. Sun, Y. Yao, X. Fan, D. Zheng, Y. Luo, S. Sun, Q. Liu, L. Li, W. Chu, L. Xie, Q. Kong and X. Sun, Sci. China Mater., 2025, 68, 2756-2763.
- 43. T. Ren, Z. Yu, H. Yu, K. Deng, Z. Wang, X. Li, H. Wang, L. Wang and Y. Xu, *Appl. Catal. B: Environ.*, **2022**, 318, 121805
- 44. M. Zhang, Z. Ma, S. Zhou, C. Han, V. Kundi, P. V. Kumar, L. Thomsen, B. Johannessen, L. Peng, Y. Shan, C. Tsounis, Y. Yang, J. Pan and R. Amal, *ACS Catal.*, **2024**, 14, 11231-11242.
- 45. H. Wang, Q. Mao, T. Ren, T. Zhou, K. Deng, Z. Wang, X. Li, Y. Xu and L. Wang, ACS Appl. Mater. Interfaces, 2021, 13, 44733-44741.
- 46. W. Fu, Z. Hu, Y. Zheng, P. Su, Q. Zhang, Y. Jiao and M. Zhou, Chem. Eng. J., 2022, 433, 133680.
- 47. W. Fu, Y. Du, J. Jing, C. Fu and M. Zhou, Appl. Catal. B: Environ., 2023, 324, 122201.
- 48. G. Wang, C. Wang, X. Tian, Q. Li, S. Liu, X. Zhao, G. I. N. Waterhouse, X. Zhao, X. Lv and J. Xu, *Small*, **2024**, 20, e2311439.
- 49. F. Yao, M. Jia, Q. Yang, F. Chen, Y. Zhong, S. Chen, L. He, Z. Pi, K. Hou, D. Wang and X. Li, *Water Research*, **2021**, 193, 116881.
- 50. Z. Chen, Y. Zhao, H. Huang, G. Liu, H. Zhang, Y. Yan, H. Li, L. Liu, M. Liu, D. Wang and J. Zeng, *J. Am. Chem. Soc.*, **2025**, 147, 18737-18746.
- 51. Q. Li, Y. Hou, J. Yin and P. Xi, Catalysts, 2023, 13, 1384.
- 52. Z. Fan, C. Cao, X. Yang, W. Yuan, F. Qin, Y. Hu, X. Sun, G. Liu, Y. Tian and L. Xu, *Angew Chem. Int. Ed.*, **2024**, 63, e202410356.
- 53. T. Li, C. Tang, H. Guo, H. Wu, C. Duan, H. Wang, F. Zhang, Y. Cao, G. Yang and Y. Zhou, *ACS Appl. Mater. Interfaces*, **2022**, 14, 49765-49773.

54. Q. Hu, S. Qi, Q. Huo, Y. Zhao, J. Sun, X. Chen, M. Lv, W. Zhou, C. Feng, X. Chai, H. Yang and C. He, *J. Am. Chem. Soc.*, **2024**, 146, 2967-2976.

55. L. Wang, C. Zhang, Z. Cao, G. Zeng, J. Liu and S. Ye, Adv. Funct. Mater., 2024, 34, 240667

## A table of contents entry

Highly active and stable Cu-doped  $\text{Co}_3\text{O}_4$  electrocatalysts were engineered using MOFs template. Tandem sites of Cu and Co could selectively catalyze reduction of  $\text{NO}_3^-$  to  $\text{NH}_3$ .  $\text{Cu}^{2+}$  facilitated adsorption and conversion of  $\text{NO}_3^-$ , inhibited HER, constructed faster electron transfer channels, achieved  $\text{NH}_3$  yield rate of 7.25 mg h<sup>-1</sup> cm<sup>-2</sup> and Faradaic efficiency of 95%.

